



Preliminary insights from hydrological field monitoring for the evaluation of landslide triggering conditions over large areas

Luca Schilirò¹ · Gian Marco Marmoni² · Matteo Fiorucci^{2,3} · Massimo Pecci⁴ · Gabriele Scarascia Mugnozza²

Received: 2 November 2022 / Accepted: 19 May 2023
© The Author(s) 2023

Abstract

Rainfall-induced landslides represent a major threat to human activities, and thus an improved understanding of their triggering mechanisms is needed. The paper reports some preliminary inferences on this topic, based on the data recorded over a 2-year period by a multi-parametric monitoring station located on one of the slopes of the Monterosso catchment (Cinque Terre, north-western Italy). This catchment has experienced multiple, concurrent shallow landslides after intense rainfall events. After defining a soil hydraulic model through data interpretation and numerical simulations, slope stability analyses were performed to elucidate several aspects related to shallow landslide occurrence. Both long-term climate conditions and single rainfall events were simulated via physically based approaches. The findings from these simulations enabled us to assume the pattern of infiltration and quantify the impact of soil hydraulic behavior on landslide triggering conditions. In this regard, various analyses were carried out on the same triggering event both at local scale and in the overall catchment, with a view to highlighting the role of initial soil moisture and soil hysteretic behavior in slope stability.

Keywords Rainfall-induced landslides · Stability analysis · Hydraulic conditions · Physically based model · Field monitoring · Italy

✉ Luca Schilirò
luca.schiliro@cnr.it

¹ Istituto di Geologia Ambientale e Geoingegneria (IGAG), Consiglio Nazionale delle Ricerche (CNR), Via Salaria Km 29, Montelibretti, 300 – 00015 Rome, Italy

² Dipartimento di Scienze della Terra e Centro di Ricerca Previsione, Prevenzione e Controllo dei Rischi Geologici (CERI), Sapienza Università di Roma, Piazzale A. Moro 5, 00185 Rome, Italy

³ Dipartimento di Ingegneria Civile e Meccanica, Università degli Studi di Cassino e del Lazio Meridionale, Via G. Di Biasio 43, Cassino, 03043 Frosinone, Italy

⁴ Dipartimento per gli Affari Regionali e le Autonomie della Presidenza, Consiglio dei Ministri (DARA), Rome, Italy

1 Introduction

Rainfall-induced landslides are the most common form of landslide worldwide (e.g., Dai et al. 2003; Park et al. 2013; Chen et al. 2014; Sajinkumar and Anbazhagan 2015; Marc et al. 2018) and can cause significant economic losses and human casualties (Petley 2012; Haque et al. 2016). In the past few years, both the frequency and the number of landslide and extreme rainfall events have increased (Kirschbaum et al. 2012; Haque et al. 2019); likely due to global climate change (Froude and Petley 2018; Gariano et al. 2020). Hence, the temporal and spatial prediction of rainfall-induced landslides is an issue of growing relevance, and major efforts have been undertaken to develop and/or improve methods and tools designed for this purpose. In particular, a number of real-time early warning systems (EWSs) have recently been developed (e.g., Froese et al. 2005; Badoux et al. 2009; Anderson et al. 2011; Maskrey 2011; Genevois et al. 2018; Abraham et al. 2022) thanks to the availability of improved measuring and monitoring networks (Alfieri et al. 2012). EWSs are generally based on data collected by systems that monitor landslide triggering factors, such as rainfall and/or pore water pressure (Thiebes et al. 2014). The growing interest in EWSs is justified by the fact that, in many cases, they offer a valid solution for risk mitigation with a low environmental and economic impact (Intrieri et al. 2012). Alarm thresholds are generally defined through empirical (e.g., Aleotti 2004; Guzzetti et al. 2008; Brunetti et al. 2010; Mathew et al. 2014; Huang et al. 2015; Dikshit and Satyam 2019; Gariano et al. 2019; Tufano et al. 2019; Valenzuela et al. 2019) or physically based models (e.g., Baum et al. 2008; Liao et al. 2011; Papa et al. 2011; An et al. 2016; Mirus et al. 2018; Hsu and Liu 2019). However, such empirical thresholds have their limitations, mainly related to the need for site-specific landslide inventories and the difficulty of properly considering the complex hydrological processes occurring in slopes (e.g., effective infiltration, evapotranspiration) prior to potential triggering rainfall events (Bogaard and Greco 2018). In this regard, many authors have used antecedent precipitation measurements to determine when landslides are likely to occur, establishing a threshold based on the amount of antecedent rainfall over a specific period (e.g., Govi et al. 1985; Pasuto and Silvano 1998; Cardinali et al. 2006; Abraham et al. 2021). Nevertheless, a key difficulty lies in the definition of the period during which precipitation accumulates. According to Guzzetti et al. (2007), the relevant literature shows a significant scatter in the considered period, that is mostly ascribable to different geological–morphological and climate features, as well as to heterogeneity and incompleteness of rainfall and landslide data used to determine thresholds. Physically based models can provide more reliable results, despite the difficulty of obtaining detailed information on hydrological, morphological, and soil characteristics, especially over large areas (Merritt et al. 2003; Rosso et al. 2006; Berti et al. 2012). Indeed, by simulating the dynamic response of soil wetting, these models can determine the amount of precipitation that is needed to trigger slope failures, directly accounting for antecedent rainfall (Wilson and Wieczorek 1995; Crosta and Frattini 2003). This is why the integration of monitoring data into simplified numerical models can represent a starting point for designing efficient EWSs, as also suggested by Stähli and Bartelt (2007). With this perspective, distributed monitoring can be crucial for a suitable physically based quantification of rainfall-induced landslide scenarios.

In our study, we carried out a series of analyses focused on the assessment of landslide triggering conditions after intense rainfall events. The concept was to make use of the data recorded by an *in situ* monitoring station in order to assess the triggering process over a wide area. Starting from field monitored data, we first defined several hydraulic parameters

of the soil, with particular emphasis on those relating to its unsaturated portion, which can play a crucial role in the onset of instabilities within shallow deposits (e.g., Baum et al. 2010; Lu and Godt 2013; Bordoni et al. 2015; Jeong et al. 2017; Rahardjo et al. 2019; Gianini et al. 2022; Martino et al. 2022). Based on our results, we analyzed the slope stability conditions at a local scale via a simplified physically based approach, considering both long-term climate conditions and a specific representative rainfall event. The outcome of these analyses was then used to carry out similar analyses over a larger area using TRIGRS (Baum et al. 2008), a physically based model specifically designed for slope stability analyses at catchment scale. In this regard, the area surrounding our monitoring station (Cinque Terre, north-western Italy) is renowned for numerous landslides that have occurred over the years due to the unique physiographic and meteo-climatic features of its small coastal catchments (e.g., Cevasco et al. 2013; Brandolini et al. 2018; Raso et al. 2019; Di Napoli et al. 2021). Hence, the objective of our work was to evaluate the importance of characterizing the hydraulic behavior of soil covers, and the impact of extrapolating local results to a larger scale. At the same time, we checked whether the information inferred from hydrological field monitoring could contribute to improving basin-scale slope stability analyses.

2 The study area

The Monterosso catchment (Fig. 1a), which extends over approximately 5.5 km², lies inside Cinque Terre National Park, along the eastern Ligurian coast (north-western Italy). The area features steep (30–40°) slopes, typically carved by deep braided ephemeral streams directly discharging into the sea. These features, which are typical of recently uplifted areas (Faccini et al. 2013), are found in many coastal basins of the easternmost part of Liguria. The combination of this complex orography with the effect of the sea strongly affects the local climate. The latter is typically Mediterranean, with hot and dry summers, and mild winters, fall being the rainiest season. Nevertheless, mean annual precipitation (1033 mm) tends to increase with altitude when moving from the coast to the watershed (Pedemonte 2005). For instance, at the highest elevations of the northern part of the catchment, mean annual precipitation reaches about 1200 mm (Cevasco et al. 2015). Extreme precipitation may also occur, generally between late summer and mid-fall, owing to self-regenerating storm cells or persistent cyclonic Tyrrhenian circulation (Crosta 1998; Cevasco et al. 2009). These rainstorms typically have a short duration (<24 h), but rainfall intensities may reach or exceed values of 100 mm/h (Cevasco et al. 2015). From a geological point of view, the local bedrock is chiefly composed of a sandstone–claystone flysch and of a pelitic complex, which is overlain by a thin (0.5–3.5 m) regolith cover. The local shallow soils and debris covers have been largely reworked over the centuries for agricultural purposes, resulting into widespread terraced areas (Fig. 1c). These represent the most iconic feature of Cinque Terre National Park (Giordan et al. 2020; Pepe et al. 2020).

However, over the last century, the terraces have been progressively abandoned and covered by Mediterranean scrub, becoming landslide-prone areas. Additionally, also in currently cultivated terraced areas a limited maintenance of the drainage systems can be observed, making the hillslopes even more susceptible to landslide occurrence (Schilirò et al. 2017). In this respect, mention may be made of at least two major rainfall events. The first occurred on the night between October 2 and 3, 1966 when heavy rainfall caused severe injuries to people and damage to buildings and infrastructure, especially in the village of Monterosso. Based on available information, the central roads

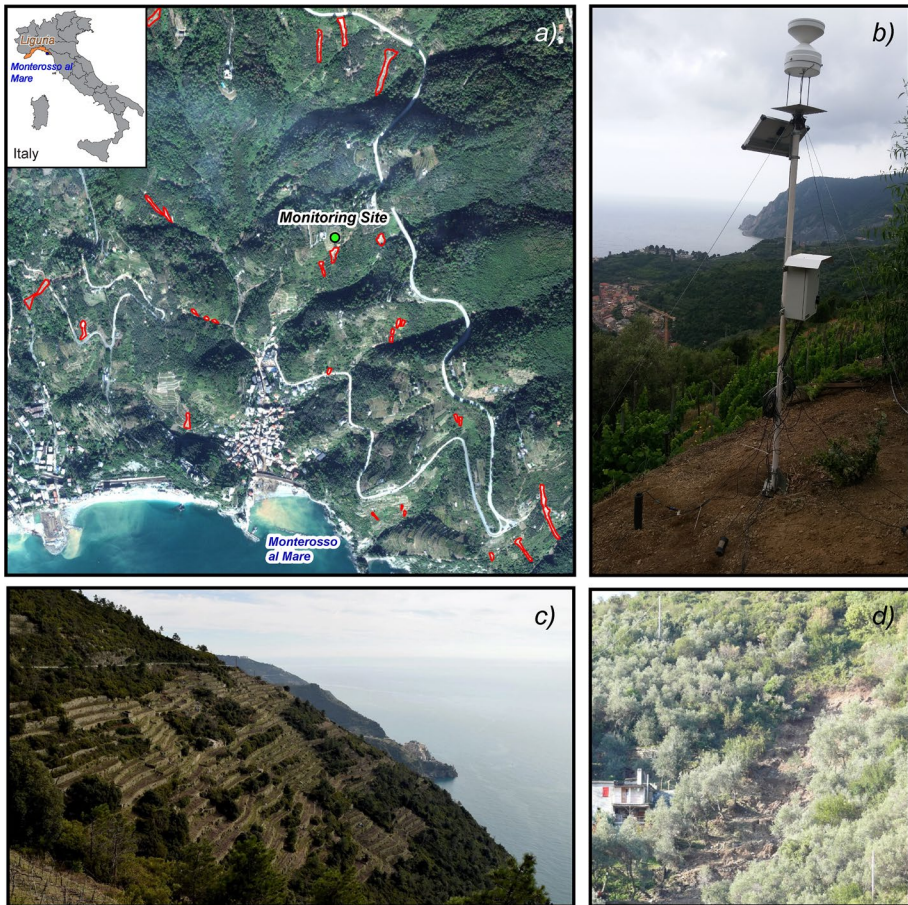


Fig. 1 **a** Distribution of the shallow landslides that occurred in the Monterosso catchment on October 25, 2011 (red polygons); the green dot indicates the location of the *in situ* monitoring station (Google Earth® satellite image); **b** picture of the monitoring station; **c** agricultural terraced area (from Di Napoli et al. 2020); **d** shallow landslide over a terraced slope (from Schilirò et al. 2018)

of Monterosso were flooded by water and debris, which spread to basements, shops, and cafes, and swept away boats lying on the beach (Guzzetti et al. 1994; Guzzetti and Tonelli, 2004). During the event, the neighboring Levanto monitoring station recorded 142 mm of rainfall, with maximum intensities of 85 mm/6 h, 127 mm/12 h, and 152 mm/24 h. The second event took place on October 25, 2011, namely between 7:00 and 17:00 UTC. The Monterosso monitoring station recorded a cumulative rainfall of 382 mm, with maximum intensities of 90 mm/h, 195 mm/3 h, and 350 mm/6 h (Regione Liguria 2012). As a consequence of this extreme event, approximately 260 shallow landslides occurred, initiating as debris slides (Fig. 2), and then, in most cases, evolving into debris avalanches or debris flows (Hungr et al. 2014). Huge amounts of earth and debris engulfed the central roads of Monterosso, reaching their maximum thickness (approximately 3 m) in the center of the village (Schilirò et al. 2018).

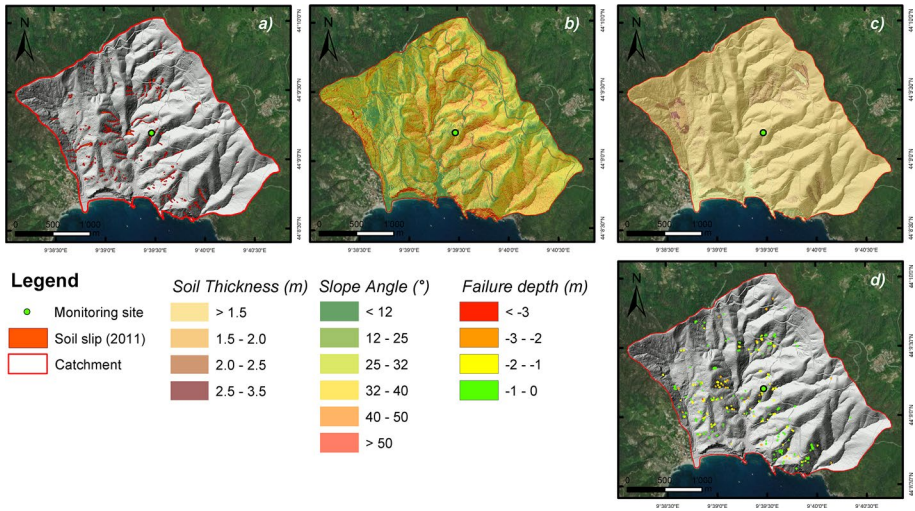


Fig. 2 Shallow soil slips observed in 2011 after the intense rainfall event (a); the slope angle (b) and soil thickness map by Schilirò et al. 2018 are also shown on a shaded relief map over the Monterosso catchment (c); the failure depth in the landslide source area was calculated by the difference between the 2011 and 2010 1 m × 1 m digital elevation models (DEMs) (d)

3 Materials and methods

3.1 The Monterosso field monitoring system

After the extreme 2011 weather event, a multi-parametric monitoring system was installed in the Monterosso catchment area, as part of an agreement between *Dipartimento per gli Affari Regionali* (DARA) of the Italian Government and *Dipartimento di Scienze della Terra* of Sapienza University of Rome, concerning research on and design of methods to quantify susceptibility to landslides in mountain areas and ability to predict them at an early stage.

The field monitoring station (Fig. 1b) is located on a south-facing vineyard terrace in the central part of the Monterosso catchment, west of the SP38 provincial road, at an elevation of 185–190 m above sea level (asl). The average slope of the terrace is 27°, but it reaches 45° on its flanks (Fig. 2b). This geometry is typical of a particular type of agricultural terrace (i.e., *cuiğa* in local dialect), whose flanks are made up of a mixture of compacted soil and rocks, in place of the more common dry-stone wall. This mixture enhances the formation of a grassy edge which, in turn, reduces runoff and erosion of the terrace flank (Martini et al. 2004). As regards soil cover characteristics, laboratory test results showed a coarse-grained (mostly gravelly) material, with minor components of low-plasticity silt and clay (Table 1). The unsaturated unit weight of soil was, instead, determined directly in the field via the sand cone method. These features are consistent with an eluvial–colluvial deposit resulting from the weathering of the underlying flysch bedrock and subsequently reworked by farming activities.

The monitoring network consists of (Fig. 3):

Table 1 Physical properties and grain-size characteristics of the soil sampled from the agricultural terrace

<i>Physical properties</i>	
Unit weight of soil solids (kN m^{-3})	26.91
Unsaturated unit weight of soil (kN m^{-3})	14.61
Degree of saturation (August 1, 2018) (%)	29.1
Porosity (%)	51.1
Liquid limit (%)	35.1
Plastic limit (%)	26.7
Plasticity index (%)	8.4
Soil type (USCS, ASTM-D2487)	GM–silty gravel
<i>Granulometric characteristics</i>	
Gravel (%)	60.2
Sand (%)	24.7
Silt (%)	11.1
Clay (%)	4.0

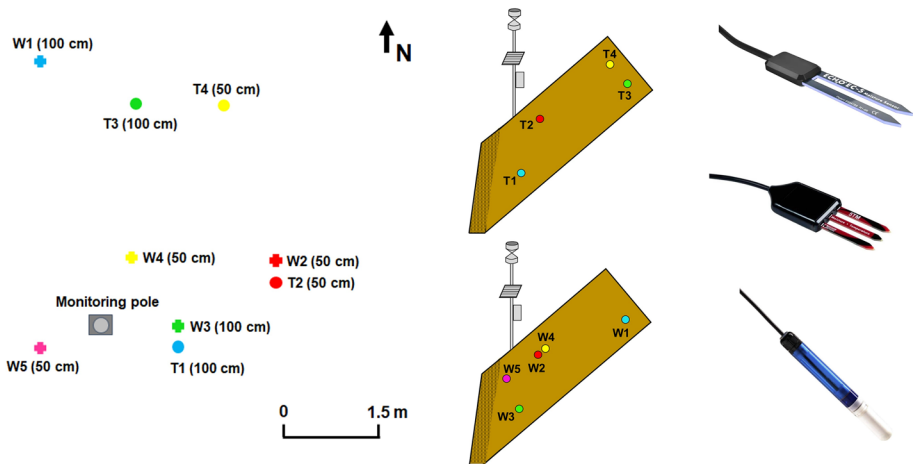


Fig. 3 Planimetric and cross section views of the monitoring system. The monitoring pole includes: rain gauge, thermo-hygrometer, power unit consisting of a solar panel equipped with a lithium battery, datalogger, and GSM/GPRS data transmission system. The depth of installation of sensors is shown in parentheses. Legend: W1–W4, sensors to measure soil volumetric water content; W5, sensor to measure soil volumetric water content and temperature; T1–4, tensiometers to measure soil water pressure. The right-hand side of the picture shows (from top to bottom) examples of ECH₂O EC-5 soil moisture sensor, ECH₂O 5TM soil moisture and temperature sensor, and tensiometer

1. 1 rain gauge (model ARG100, Campbell Scientific Inc., Logan UT);
2. 1 thermo-hygrometer (model TTU600, Tecno. El. s.r.l., Rome, Italy);
3. 4 tensiometers (T1–T4) to measure soil water pressure within the range of -85 kPa to $+100$ kPa (model T4e, UMS, München, Germany);
4. 4 sensors (W1–W4) to measure soil volumetric water content (model ECH₂O EC-5, Meter group, Pullman, WA);
5. 1 sensor (W5) to measure soil volumetric water content and temperature (model ECH₂O 5TM, Meter group, Pullman, WA).

Both the tensiometers and the soil water content sensors were installed at different locations and depths in order to assess spatial changes of hydraulic conditions over time (Fig. 3). In particular, two different depths (50 and 100 cm) were selected to investigate the vertical infiltration process within a depth range consistent with the average soil thickness estimated for terraced areas in the Monterosso catchment (Fig. 4b). In terms of planimetric position, we placed most of the sensors in the outermost part of the terrace, while three sensors (W1, T3, and T4) were installed in the part farthest from the terrace edge, with the aim of observing the hydraulic response of the soil to rainfall events along the slope dip direction.

Data was collected (sampling rate: 5 min) by a CR1000 datalogger (Campbell Scientific Inc.), powered by a photovoltaic panel equipped with a lithium battery. The power unit also feeds a data transmission system based on the GSM (Global System for Mobile Communications)/GPRS (General Packet Radio Service) technology. Specifically, data is automatically transmitted at set intervals to an external server, which can be cloud-accessed from the web. In this way, the application makes it possible not only to display and download data remotely, but also to check the operating status of the monitoring system, detecting potential failures in almost real time.

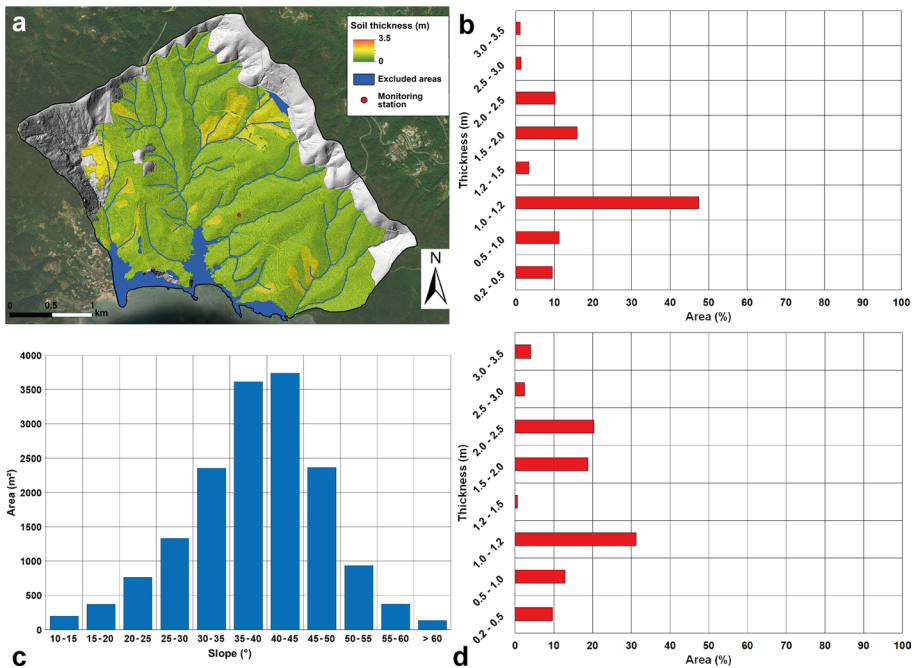


Fig. 4 **a** Soil thickness map of the Monterosso catchment clipped within the terraced areas. Areas excluded are all those (i.e., beaches, gullies, cliffs, urbanized areas) that have been excluded from soil thickness estimation (modified after Schilirò et al. 2018); **b** soil thickness distribution within the terraced areas; **c** slope distribution within the 2011 source areas; **d** soil thickness distribution within the 2011 source areas

3.2 Physically based modeling

In this work, use was made of different physically based models to reconstruct the hydraulic behavior of the agricultural terrace and its stability conditions.

For hydraulic behavior, we employed HYDRUS-1D version 4.0 (Šimůnek et al. 2008), a software package developed by USDA (United States Department of Agriculture) for simulating one-dimensional, uniform water movement in variably saturated porous media. This model, which is widely used in the literature to analyze water, solutes, and heat propagation in soil (e.g., Kanzari et al. 2018; Shekhar et al. 2019; Davis and Ekwue 2022), uses a modified form of the Richards equation for simulating water flow:

$$\frac{\partial \theta}{\partial t} = \frac{\partial}{\partial x} \left[K \left(\frac{\partial h}{\partial x} + \cos \cos \delta \right) \right] - S \tag{1}$$

where θ is the volumetric water content, t is time, h is the pressure head, S is the sink term, δ is the angle between the flow direction and the vertical axis, and K is the unsaturated hydraulic conductivity given by:

$$K(h, x) = K_s(x)K_r(h, x) \tag{2}$$

where K_r and K_s are the relative and saturated hydraulic conductivity, respectively. For the analytical hydraulic model to simulate water flow, we chose the van Genuchten–Mualem model (van Genuchten 1980), which may be summarized as follows:

$$\theta = \theta_r + \frac{\theta_s - \theta_r}{\left[1 + (\alpha |u_a - u_w|)^n \right]^{1-\frac{1}{n}}} \tag{3}$$

where θ is the volumetric water content, θ_s is the saturated water content, θ_r is the residual water content, α is a fitting parameter depending on pore-air pressure, n is a fitting parameter depending on pore size distribution, u_a is the pore-air pressure, and u_w is the pore water pressure.

As concerns slope stability, we relied on two different models depending on the scale of our analysis, namely a local-scale model and a catchment-scale model. In the former instance, we resorted to the simplified approach proposed by Lu and Godt (2008). The latter is an extended version of the conventional infinite slope model, which enables calculation of slope stability, in terms of factor of safety (FS), under partially saturated conditions according to:

$$FS = \frac{\tan \varphi'}{\tan \beta} + \frac{2c'}{\gamma H \sin 2\beta} - \frac{\sigma^S}{\gamma H} \left[(\tan \beta + \cot \beta) \tan \varphi' \right] \tag{4}$$

where φ' is the soil effective friction angle, β is the slope angle, c' is the soil effective cohesion, γ is the unit weight of soil, H is the potentially unstable soil thickness, and σ^S is the suction stress, which may be defined in terms of matric suction ($u_a - u_w$) for variably saturated materials as (Lu and Likos 2006; Lu et al. 2010):

$$\sigma^S = -(u_a - u_w) = u_w \text{ for } u_a - u_w \leq 0 \tag{5}$$

$$\sigma^S = -\frac{(u_a - u_w)}{\left[\alpha (u_a - u_w) \right]^{\frac{(n-1)}{n}}} \text{ for } u_a - u_w > 0 \tag{6}$$

Lu et al. (2010) also proposed a formula for calculating suction stress considering the equivalent degree of saturation (S_e):

$$\sigma^S = -\frac{S_e}{\alpha} \left(S_e^{1-n} - 1 \right)^{\frac{1}{n}} \text{ with } S_e = \frac{\theta - \theta_r}{\theta_s - \theta_r}. \tag{7}$$

Thus, taking into account the two formulas for calculating σ^S , the factor of safety can be predicted on the basis of both soil water content and pore water pressure values, considering parametrically two different slope angles, 27° and 38°, representing the slope angle of the monitored terrace and the mean slope angle of the 2011 failed slope (Fig. 4c), respectively.

For the catchment-scale analysis, we used TRIGRS (Baum et al. 2008), a model developed by the United States Geological Survey (USGS) that is largely used to predict rainfall-induced landslides over large areas (Weidner et al. 2018; Park et al. 2019; Ávila et al. 2021; Schilirò et al. 2021; Tran et al. 2022). TRIGRS is a model that combines two calculations: (i) a one-dimensional analytical solution for pore pressure response to rainfall infiltration, and (ii) an infinite slope stability calculation. The infiltration model, based on a linearized solution of the Richards equation proposed by Iverson (2000), can account for different types of rainfall inputs on the ground surface. In response to these inputs, TRIGRS can compute the transient pressure head response $\psi(Z,t)$ based on various input parameters, such as slope, soil thickness, depth of the initial steady-state water table, and saturated hydraulic conductivity. At each time step, TRIGRS simulates the rise of the water table if the amount of infiltrating water reaching the surface exceeds the amount that gravity can drain. This analysis is performed by comparing the excess water volume with the pore space directly above the water table, and by applying the resulting water weight at the initial top of the saturated zone at each time step (Baum et al. 2010). Then, the factor of safety is determined at a specific depth Z using the following formula:

$$FS = \frac{\tan \varphi'}{\tan \beta} + \frac{c' - [\psi(Z,t)\gamma_w \tan \varphi']}{\gamma Z \sin \beta \cos \beta} \tag{8}$$

The model can also account for infiltration into a partially unsaturated surface layer above the water table. In this instance, TRIGRS linearizes the Richards equation by using a number of hydrodynamic parameters, as suggested by Gardner’s hydraulic model (1958). In the unsaturated configuration, the pressure head takes into account an effective stress parameter, which is equal to S_e (Vanapalli and Fredlund 2000).

To use the TRIGRS model in our study, we relied on a prior analysis (Schilirò et al. 2018), representing the instability scenario arising from the 2011 event in the overall Monterosso catchment. We updated this analysis keeping the input parameters unaltered, except for those concerning the unsaturated phase, whose values were replaced with those obtained in our study. By so doing, we were able to check whether calibrating these parameters with field data could help better define landslide occurrence over large areas. For the spatial resolution of the input data, we selected 4 m × 4 m, which turned out to be the optimal resolution for performing this type of analysis (Schilirò et al. 2018).

Simulation results, expressed in terms of factor of safety (FS) map, were compared with the source areas of the landslides triggered during the event (Fig. 2). To quantify the predictive performance of the model, we carried out an receiver operating characteristic (ROC) curve analysis for different thresholds (i.e., different FS values). This analysis relates the true positive rate (TPR), which is the number of “landslide” cells that are

correctly predicted, to the false positive rate (FPR), which is the number of “stable” cells that are erroneously simulated as unstable. The area under the curve (AUC) is the parameter that typically quantifies the performance of the model: the larger the value, the better the prediction.

4 Results

4.1 Analysis of field monitoring data

We analyzed the data recorded by the monitoring station from August 1, 2018 to September 30, 2020. During this period, data was continuously acquired, except for breakdowns of individual sensors and short interruptions due to temporary outage of the power supply system. As regards the rainfall regime (Fig. 5a), several intense, short-duration events were recorded during summer and fall, corresponding to the Mediterranean climate. The most significant event occurred between October 27 and 29, 2018, when approximately 225 mm of rainfall were recorded in just three days (159 mm on October 29 itself). This event also showed extremely high hourly rainfall peaks, with a reached maximum value of 66.8 mm. Rainfall directly induced sudden drops in the air and soil temperatures (Fig. 5b); however, a clear seasonal trend was observed. It is interesting to note that the air temperature had more significant daily changes than soil temperature, which reached approximately 30 °C in summer and 10 °C in winter.

As regards hydraulic monitoring, the data recorded by tensiometers (Fig. 5c) showed very high matric suction values (i.e., negative soil water pressure) under hot dry summer conditions (drying periods). These values, reaching up to −900 hPa at the deepest sensor (T1), became approximately equal to zero immediately after the first fall rains, and were mostly unchanged until the next summer (wetting periods). Moreover, soil moisture records showed a clear relation with rainfall peaks (Fig. 5d). However, the deepest sensor (i.e., W1) recorded lower values (0.05 to 0.15) than the others (0.10 to 0.3).

If the spatial distribution of sensors is considered (Fig. 3), we can notice that those located downslope (i.e., W5 and W3) generally recorded higher water content values than the sensor located upslope at the same depth (i.e., W2–W4 and W1).

During one of the most important rainfall events (July 27–28, 2019), T2 and T4 were the first sensors to detect a significant pore water pressure change, approximately one hour after the first rainfall peak, given their position closer to the surface (Fig. 6). In contrast, T1 showed a sharp decrease in matric suction only at 3:00 am on July 28, when both T1 and T2 recorded their maximum values. T3, the deepest sensor upslope of the terrace, started to record pore water pressure changes only at 6:00 am on July 28, reaching maximum values approximately six hours later.

4.2 Reconstruction of the soil hydraulic behavior via numerical modeling

The data recorded over a two-year timespan made it possible to reconstruct the hydraulic behavior of the investigated soil in a comprehensive way, considering extremely variable atmospheric conditions. As mentioned above, this behavior was strongly related not only to the saturated phase but also to the unsaturated one. The analysis of unsaturated hydraulic properties is usually performed by reconstructing soil water characteristic curves (SWCCs), which describe the relationship between volumetric water content and matric

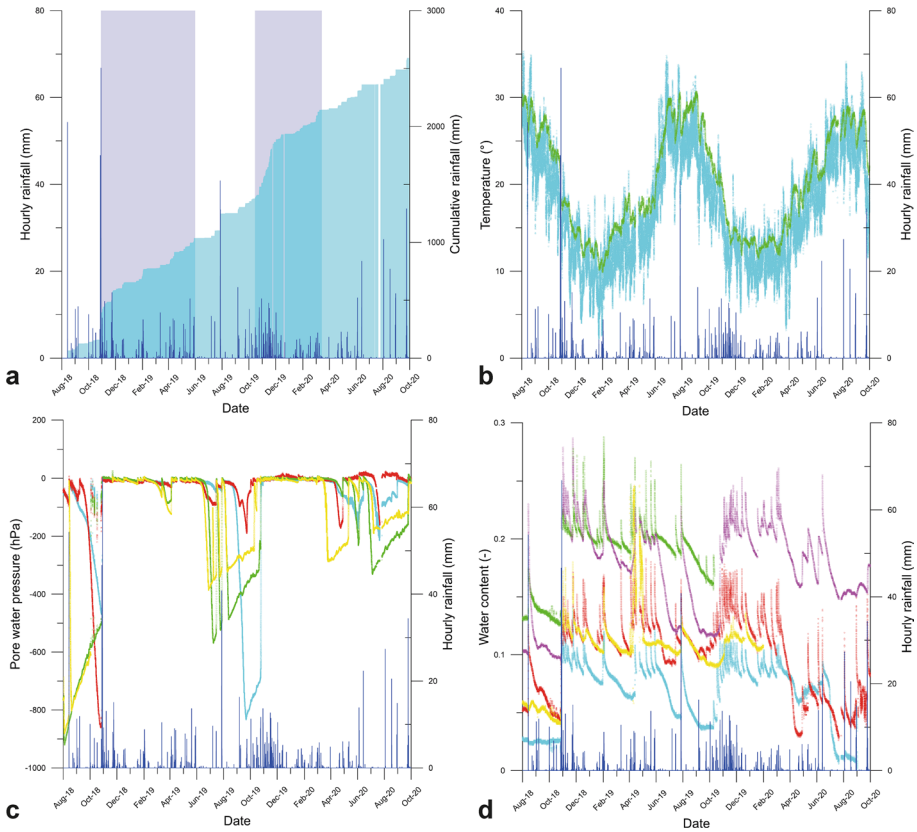


Fig. 5 Data recorded by the monitoring station from August 1, 2018 to September 30, 2020: **a** hourly and cumulative rainfall; drying and wetting periods are also highlighted; **b** soil and air temperature; **c** soil water pressure at different locations; **d** soil water content at different locations

suction. In this study, different SWCCs were determined in the upper (0–50 cm) and lower (50–100 cm) parts of the soil profile by coupling the records of T2–W2 and T1–W3, respectively. In particular, use was made of the nonlinear least-square method (Kemmer and Keller 2010) for fitting Eq. 3 to soil moisture–pore water pressure values, in order to determine the unknown parameters α and n . However, SWCCs can exhibit a hysteretic behavior depending on soil wetting and drying (Fredlund et al. 2011; Likos et al. 2013; Yang et al. 2019). In wetting periods, the volumetric water content induced by rainfall infiltration corresponded to a specific water pressure value, which was lower than that resulting from the same soil moisture level in drying periods. This type of process can notably affect the unsaturated shear strength of soils (Kristo et al. 2019). Thus, for each pair of sensors, we reconstructed a drying and wetting curve in relation to the period of the year in which the data had been recorded (Fig. 7). Some data scatter was observed; as also pointed out by Bordoni et al. (2015), this scatter can be correlated with very rapid hysteresis processes occurring after more intense rainfall events. Fitting parameters (Table 2), especially those concerning the wetting process of the lower soil portion, showed particularly high values, which can be explained by the presence of gravel in the investigated soil (Yang et al. 2019). To assess the effectiveness of the fitting procedure, we calculated the root mean square

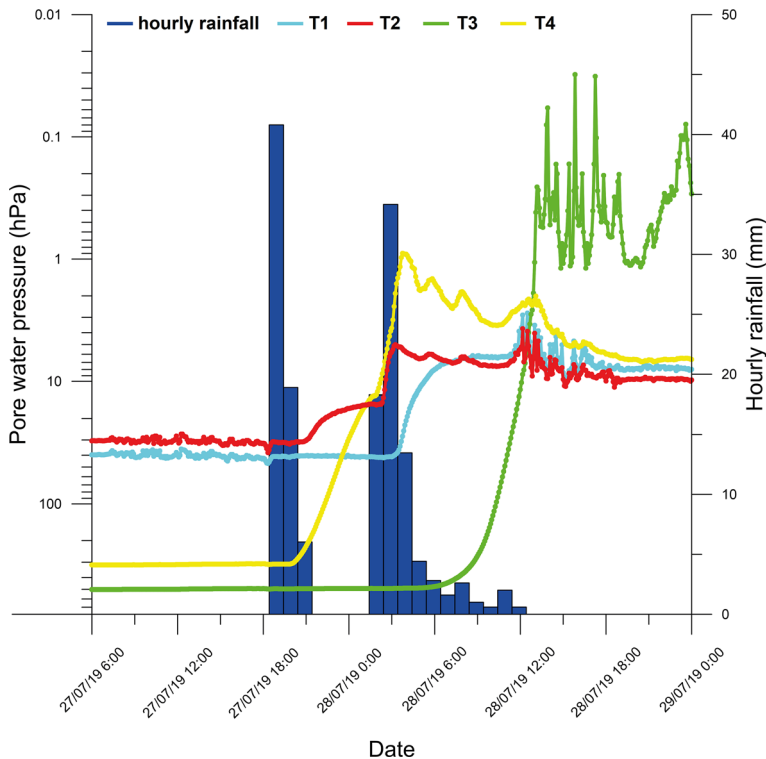


Fig. 6 Soil water pressure values recorded by the four tensiometers during the July 27–28, 2019 rainfall event

error (RMSE) for each of the four curves obtained. The resulting RMSE values were fairly low, ranging between 0.004 and 0.008 (Table 2), thus substantiating the reliability of the fitted curves.

After defining the SWCCs of the upper and lower soil portions, we used the resulting fitting parameters as input data to the HYDRUS-1D model. More particularly, we first carried out a numerical simulation over a six-month period (i.e., August 1, 2018–January 31, 2019) to calibrate the α values, together with the saturated hydraulic conductivity under drying (K_{sd}) and wetting (K_{sw}) conditions. A subsequent simulation considered the remaining period (i.e., February 1, 2019–September 30, 2020), in order to validate all of the hydraulic parameters, with a view to using them in the following slope stability analyses (Sect. 4.3). In the latter simulation, we used W2 and W3 as control points of volumetric water content, while in the first simulation we employed both water pressure and water content data for calibrating the above-mentioned parameters via inverse optimization. A 100-cm soil profile inclined by 27° was chosen as geometric configuration of the investigated soil profile. A free drainage condition was considered along the bottom boundary, while hourly data was used as rainfall input. Evapotranspiration was accounted for by using daily maximum and minimum temperature records within the Hargreaves equation (Jensen et al. 1997).

The results of parameter calibration revealed that the lower part of the soil had a higher K_{sd} value than the upper one (1.16×10^{-5} vs. 9.49×10^{-6} m/s), while K_{sw} was equal

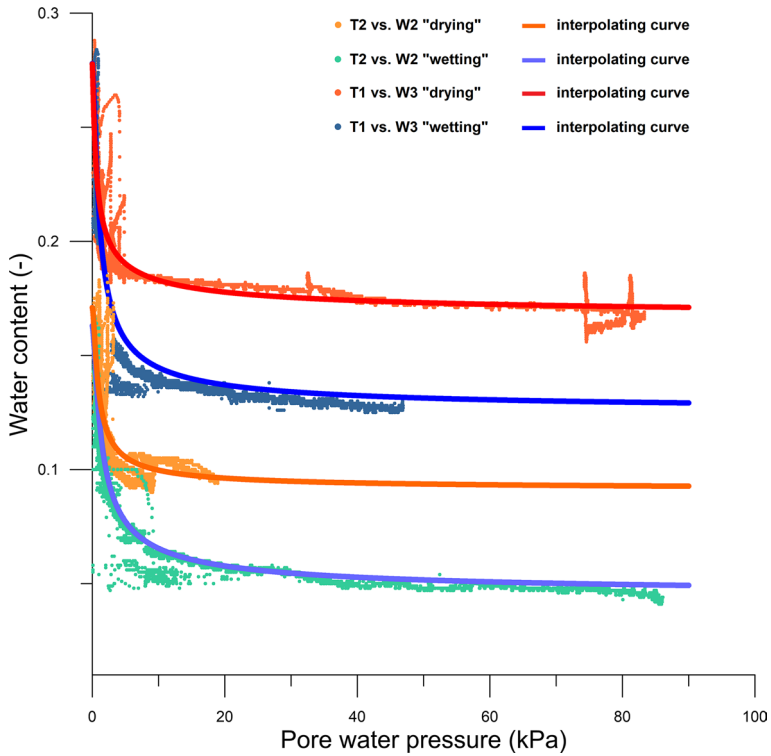


Fig. 7 SWCCs resulting from the interpolation of T2–W2 and T1–W3 data recorded in wetting and drying periods (see Fig. 5a)

Table 2 Parameters of van Genuchten–Mualem model obtained from the fitting procedure of T2–W2 and T1–W3 data

<i>Upper soil (0–50 cm) T2 versus W2</i>			
α_d (cm ⁻¹)	0.177 (0.194)	α_w (cm ⁻¹)	0.329 (0.222)
n_d (-)	1.741	n_w (-)	1.767
θ_{sd} (-)	0.171	θ_{sw} (-)	0.163
θ_{rd} (-)	0.091	θ_{rw} (-)	0.044
RMSE (-)	0.008	RMSE (-)	0.004
<i>Lower soil (50–100 cm) T1 versus W3</i>			
α_d (cm ⁻¹)	0.278 (0.452)	α_w (cm ⁻¹)	0.828 (0.414)
n_d (-)	1.495	n_w (-)	1.706
θ_{sd} (-)	0.278	θ_{sw} (-)	0.278
θ_{rd} (-)	0.165	θ_{rw} (-)	0.125
RMSE (-)	0.007	RMSE (-)	0.006

The “d” and “w” subscripts indicate “drying” and “wetting” parameters, respectively. The values in parentheses show the parameter value after calibration with HYDRUS

to 6.94×10^{-6} m/s in both cases. The results of the comparison between modeled and recorded water content values (Fig. 8) were in a good agreement for both the upper and lower parts of the soil profile during most of the investigated period. The most significant

inconsistencies were observed in the first (August–October 2018) and last (April–October 2020) parts of the monitoring survey; the RMSEs calculated over the entire period were rather small both in the upper (RMSE: 0.031) and lower (RMSE: 0.029) soil portions.

4.3 Slope stability analyses

After validating the hydraulic parameters of the soil on a preliminary basis, we reconstructed slope stability conditions through the simplified approach described in Sect. 3.2. As mechanical parameters of the soil, we used a friction angle of 31° (Schilirò et al. 2018), while effective cohesion was assumed to be equal to zero, considering the high degree of soil remolding associated with farming practices.

As a first step, we calculated FS over the entire monitoring period in order to check the potential onset of instability conditions at depths of 50 and 100 cm. To define suction stress (σ^S), we generally used Eq. 7 with data recorded by W2 and W3. For near-saturation conditions only, we directly used positive water pressure values recorded by T1 and T2. It is worth pointing out that, in line with the above, we used the “wetting” parameters of van Genuchten–Mualem model during wetting periods, and vice versa. The resulting trends (Fig. 9) showed that FS always lays above 1, which is consistent with field evidence during the two years of observation. The trend was more stable at a depth of 100 cm, whereas the upper part of the soil had larger FS changes depending on its rapid water content

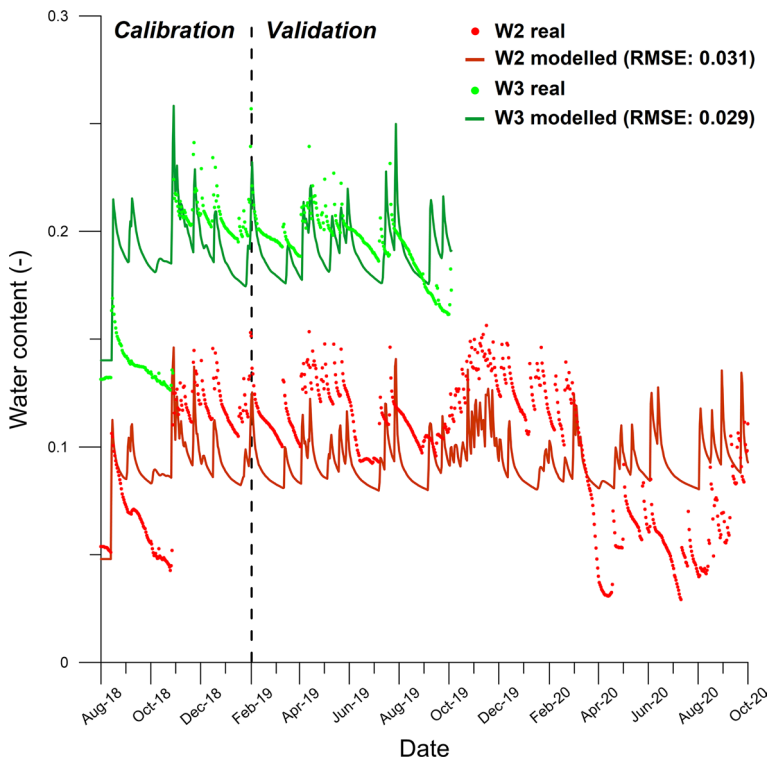


Fig. 8 Comparison between recorded (dots) and modeled (lines) soil water content at depths of 50 cm (W2) and 100 cm (W3)

fluctuations. In other words, individual rainfall events were supposed to cause sudden and significant FS drops even during spring–summer periods, when the highest FS values were reached. In winter, the FS trend at a depth of 50 cm was variable, but within a smaller range.

The same approach was taken to reconstruct slope stability conditions at local scale during the rainfall event that took place on October 25, 2011 (see Sect. 2). In this instance, hydraulic conditions were reconstructed with HYDRUS simulations, employing the calibrated model described in the preceding section. We first evaluated the initial soil moisture conditions (i.e., prior to the intense rainfall event) through a numerical simulation using daily rainfall data in the previous month. Afterward, FS was calculated during the event (7:00–17:00 UTC) using hourly rainfall data provided by ARPAL (*Agenzia Regionale di Protezione dell’Ambiente Ligure*). Results (Fig. 10a) indicate that FS at a depth of 50 cm rapidly diminished after 9:00 UTC (start of the most critical stage of the rainfall event) and reached a value of less than 1 at 11:00 UTC. Conversely, the reduction of FS at a depth of 100 cm was less marked and started about one hour later (10:00 UTC). Also in this instance, the most critical value was attained at 11:00 UTC, but it remained above 1 (i.e., 1.18). At the end of rainfall, FS tended to increase in both cases, with a greater gradient at a depth of 50 cm.

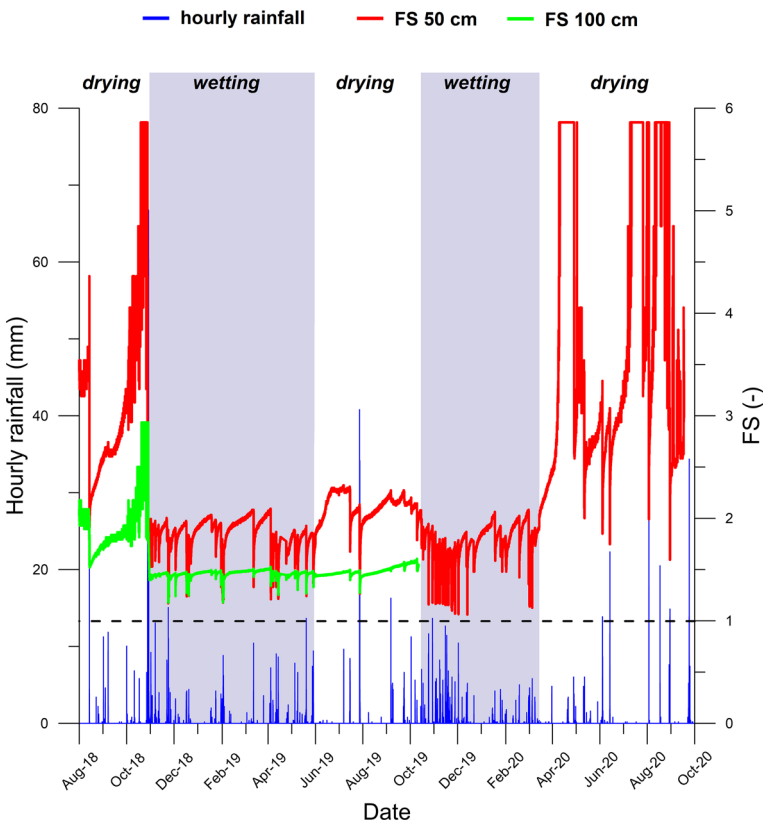


Fig. 9 Trend of the factor of safety (FS) at depths of 50 cm and 100 cm vs. hourly rainfall between August 1, 2018 and September 30, 2020

Nevertheless, the local conditions of the investigated slope did not represent the overall Monterosso catchment. This is why different results can be achieved when considering a slope angle of 38° (i.e., the average slope angle measured in the 2011 landslide source areas; see Fig. 4c).

By replacing this value with the preceding one (27°), representing the monitored terraced slope, we observed that critical conditions also arose at a depth of 100 cm as early as at 10:00 UTC (Fig. 10b). Taking into account that soil thickness in source areas was equal to or greater than 1 m (Fig. 4d) on average, we concluded that, also in this instance, simulation results were consistent with field evidence.

After local-scale analysis, we decided to simulate the 2011 event in the overall Monterosso catchment using the TRIGRS model. Results highlighted a good agreement between TRIGRS cells at $FS < 1$ and the location of landslides (Fig. 11). This performance was corroborated by the area under curve (AUC) metrics obtained from the ROC (receiver operator characteristic) curve; the latter returned a value of 79.3% (Table 3), given by a reduced number of false positives and the absence of landslides above $FS > 2$.

5 Discussion

The data recorded by tensiometers and water content sensors (Fig. 5c, d) yielded some preliminary indications about the hydrological behavior of the soil. In the first place, the lag time between rainfall events and hydraulic changes was very low, which is consistent with the hydraulic conductivity typical of coarse-grained materials (Table 1). We identified an upper soil portion (0–50 cm) with a K_{sd} value of 9.49×10^{-6} m/s, whereas the lower part (50–100 cm) was slightly more permeable (1.16×10^{-5} m/s). As regards the parameters of the unsaturated phase (Fig. 7 and Table 2), the difference between the two parts proved to depend on the different distribution of pore sizes as a function of depth, which might in turn be correlated with grain-size changes. The high α values obtained in the bottom part suggested the presence of material with larger pores. The latter may be ascribed to the method used to build farming terraces in Cinque Terre, which involves the upslope excavation of the filling material. The geometry of the terrace could also explain the differences

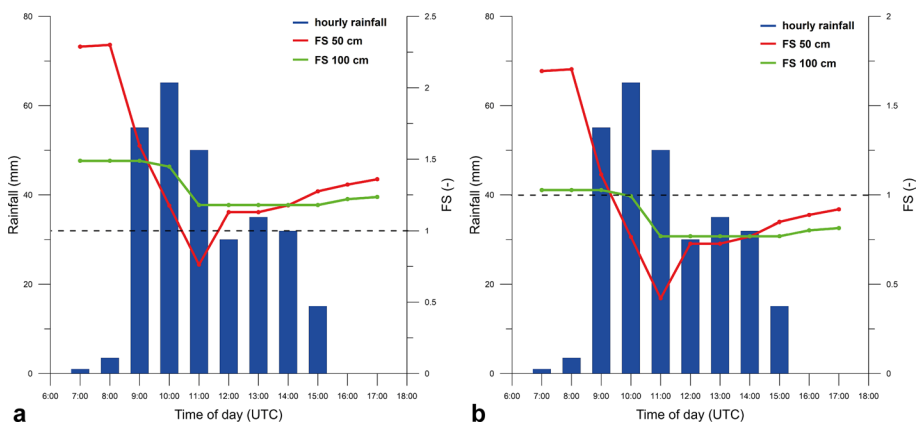


Fig. 10 FS trend at depths of 50 cm and 100 cm vs. hourly rainfall during the October 25, 2011 event, assuming slope angles of 27° (a) and 38° (b)

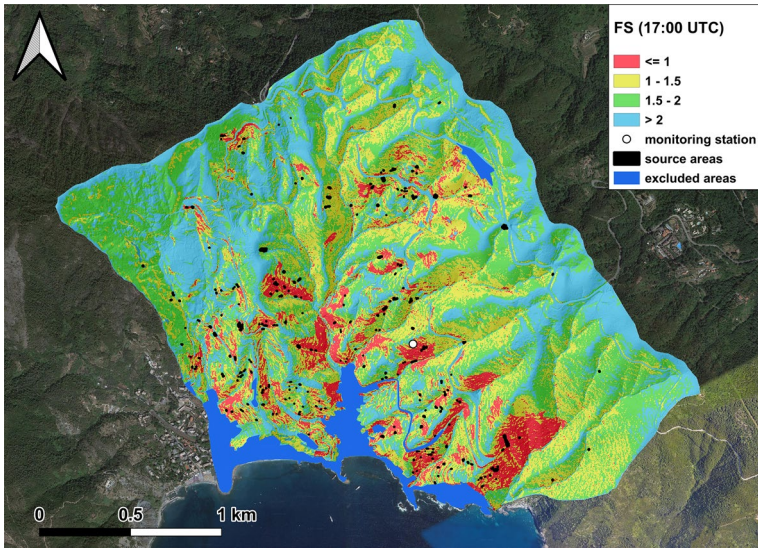


Fig. 11 FS map of the Monterosso catchment at the end of the October 25, 2011 event (17:00 UTC) based on the simulation carried out with the TRIGRS model

Table 3 True positive rate (TPR), false positive rate (FPR), and area under curve (AUC) values resulting from a comparison between the FS map obtained with TRIGRS and the 2011 landslide source areas

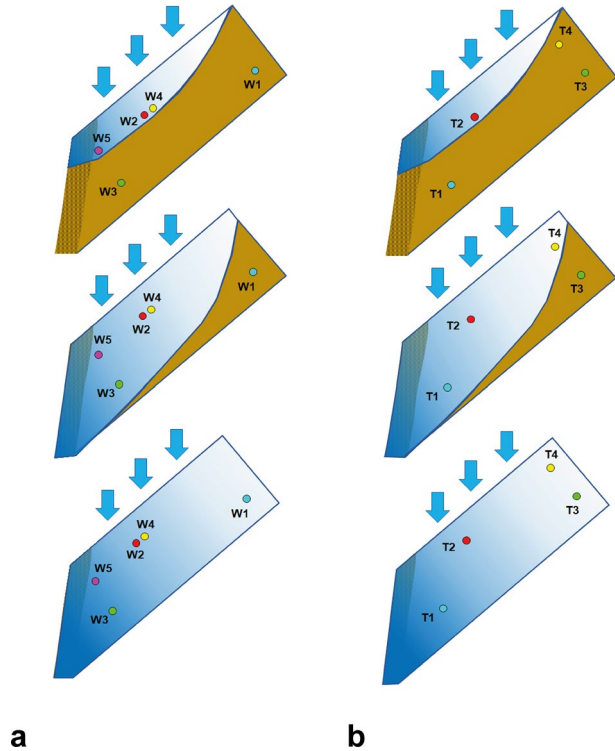
Simulation	TPR (%)	FPR (%)	AUC (%)
Our analysis	42.4	0.09	79.3
Schilirò et al. (2018)	49.5	18.2	74.8

The table also displays the same parameters obtained in a similar analysis described in Schilirò et al. (2018)

in water content trends. The results shown in Figs. 5 and 6 best represent a wetting front infiltration scheme (Schilirò et al. 2019), in which a reduction of matric suction first occurs in the upper part of the soil and, if rainfall persists, positive pore water pressures can also develop (Fig. 12a) due to the accumulation of infiltrating water on the edge of the terrace (Fig. 12b). In this respect, we are aware that a detailed description of this process should include an evaluation of the role of the terrace flank, which probably acts as a low permeability boundary. However, this would require a 2D–3D analysis going beyond the scope of this work. In fact, the main objective of our study was to better define the hydraulic parameters of the soil based on recorded data and then use them in slope stability analyses at catchment scale. Nevertheless, in the light of data collected during specific rainfall events, we deemed it reasonable to assume the above-described infiltration scheme.

With regard to slope stability, the analysis performed over the two-year monitoring period showed strong FS changes upon significant rainfall peaks and/or prolonged rainfall periods (Fig. 9). These changes were more marked in the shallowest part of the soil, where the contribution of partial saturation to soil shear strength was higher. During the investigated period, no landslide phenomena were recorded in the area, which agrees with the absence of FS values below 1 in the modeling results. By contrast, during the

Fig. 12 Wetting front infiltration scheme considering the presence of: **a** soil water content sensors, and **b** tensiometers. The blue arrows represent rainfall input



2011 event, the slope accommodating the monitoring station experienced very shallow failures. The latter evidence was consistent with the outcome of numerical simulations, which confirmed that FS was below 1 at a depth of 50 cm, upon the 11:00 UTC rainfall peak, whereas the FS reduction at a depth of 100 cm was not sufficient to induce instability (Fig. 10a).

After these analyses, we decided to simulate the 2011 event once again, with the slope conditions of the investigated terrace, but assuming a change in initial soil moisture, with a view to gaining further insight into its role in the onset of failure under the same triggering event. Considering that HYDRUS simulations returned an initial S_e equal to 0.45 at the beginning of the October 25, 2011 event, we selected drier (S_e : 25%) and wetter (S_e : 75%) initial conditions in slope stability calculation, referring to a mean slope angle of 27°. At the same time, we used both “drying” and “wetting” retention curve parameters (Table 2) to also quantify the effect of the hysteretic behavior of the soil. The resulting trends showed, once again, that the highest FS changes occurred in the upper part of the soil, where the initial FS value dropped by about 1, passing from S_e 25% to 75% (Fig. 13a). It is also worth noting that the use of “wetting” parameters significantly reduced stability, especially with an initial S_e of 25%. In the latter instance, the reduction was sufficient to induce failure at 11:00 UTC, as in the other instances featured by a higher S_e . This finding stresses the importance of considering not only existing soil moisture conditions, but also the proper soil hysteresis path in relation to the season in which the rainfall event occurs.

As regards FS at a depth of 100 cm (Fig. 13b), the differences with variable initial soil moisture and “drying”/ “wetting” parameters were less pronounced, and failure

conditions were never reached. This point can be explained by the infiltration scheme inferred from recorded data and replicated in HYDRUS simulations i.e., the advance of the wetting front. As stated above, the presence of a wetting front moving downward during intense rainfall events develops positive pore water pressures mostly in the shallowest part of the soil. These pressures become progressively lower with depth, where the instability process mainly depends on the loss of matric suction. This means that the lower part of the soil is less susceptible to failure, unless other types of hydraulic processes take place (i.e., temporary water table rising). The data recorded by the monitoring station did not allow us to hypothesize this type of process. However, it is worthwhile emphasizing that only rainfall data was available for the most significant rainfall event that occurred in the investigated period (October 27–29, 2018). Indeed, the hydraulic data of the soil was not collected during the event due to a temporary failure of the sensors. Hence, the formation of a perched water table cannot be excluded a priori.

As regards the reconstruction of the 2011 landslide events in the overall Monterosso catchment via TRIGRS, the good performance of our simulation was confirmed by the AUC value, which was higher than that obtained in a similar analysis carried out by Schilirò et al. 2018 (Table 3). The improvement was related to the FPR value, which was much lower in the new analysis. Specifically, our analysis predicted a reasonable percentage of source areas (42.4%) with a very low number of false positives. Conversely, although the previous analysis correctly simulated a slightly higher percentage of landslides (49.5%), the extent of areas erroneously predicted as “unstable” was much larger (Fig. 14a). This means that the use of updated hydraulic parameters improves the performance of the model. Furthermore, a strong reduction in false alarms is certainly welcomed in view of the potential application of the model in EWSs.

Finally, it is important to stress that the above-described insights rely on interpretation of field monitoring data and simplified modeling as part of a wider and still ongoing research activity. The next step will be the confirmation of the hypothesized infiltration scheme (Fig. 12) via 2D–3D numerical analyses, in order to account for spatial changes in the hydraulic properties of the soil across the terrace, with particular regard to its flanks. These analyses will be supported by an in-depth physical and hydraulic characterization of

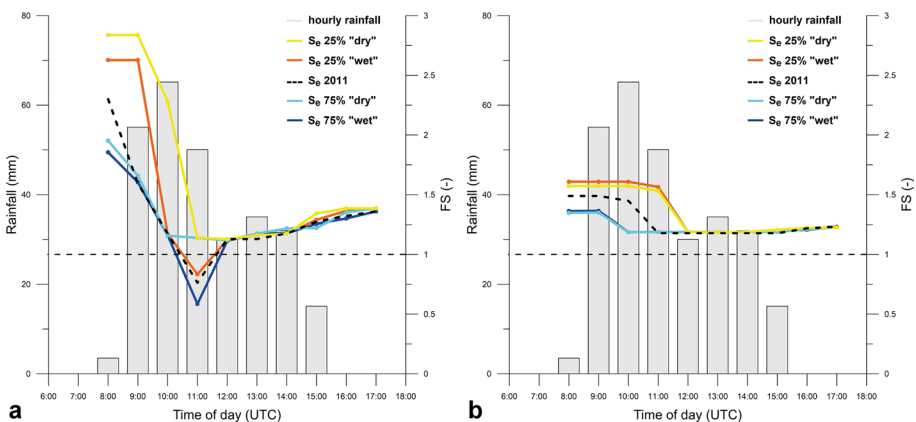


Fig. 13 FS trends at depths of 50 cm (a) and 100 cm (b), calculated during the October 25, 2011 event, assuming different initial soil moisture conditions (in terms of S_e) and “drying”/ “wetting” parameters

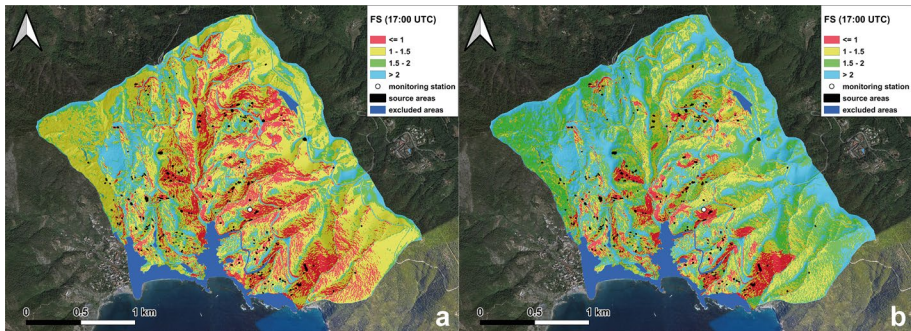


Fig. 14 FS maps of the Monterosso catchment at the end of the October 25, 2011 event (17:00 UTC) based on the simulation performed by Schilirò et al. 2018 (a), and after our update of hydraulic parameters (b)

the terrace in different sectors, alongside with a series of laboratory flume tests. The latter will be conducted on a soil slope model reproducing field conditions, following the procedure described in Schilirò et al. 2019. The results of the planned activities will provide useful information to enhance the reliability of analyses over large areas.

6 Conclusions

In this paper, we have presented and analyzed the data recorded by an *in situ* monitoring station located in the Monterosso catchment, making part of Cinque Terre National Park, in northern Italy. The aim of our study was to obtain some preliminary insights into the hydraulic behavior of soil covers and shallow landslide triggering mechanisms, to be used as a basis for stability analyses over large areas. Starting from atmospheric data and soil hydraulic data collected over a two-year period, we first built a hydraulic model of the soil, paying particular attention to characterizing its unsaturated phase. The resulting model, consisting of an upper and lower part (both with hydraulic parameters typical of coarse-grained materials), was obtained from numerical simulations with HYDRUS. The simulations also allowed us to infer the advance of a wetting front as a potential infiltration scheme. As regards landslide triggering conditions, local-scale stability analyses showed that the strongest FS changes occurred in the upper part of the soil, where the loss of matric suction was faster and the development of positive pore water pressures more pronounced. Simulation of the October 25, 2011 event emphasized the major role of initial moisture and hysteretic behavior of the soil, as well as local slope angle, in slope stability conditions. The same event was modeled at catchment scale. In the latter modeling exercise, the use of parameters calibrated with field data improved the predictive performance of the TRIGRS model vs. prior analyses carried out in the same area. This evidence stressed the importance of hydraulically characterizing weathered soil covers that are landslide-prone, with a view to designing more reliable future scenarios. In view of the above, future efforts will be devoted to an in-depth physical and hydraulic characterization of the investigated slope, taking into account potential spatial changes in soil parameter values in relation to the geometry of terraces. These efforts will hopefully enable us to refine and improve the hydraulic model of the soil discussed in this paper and to better define potential conditions for rainfall-triggered shallow landslides initially at local scale and then in the overall

catchment. Therefore, this work should be considered as a first attempt to couple field monitoring data with simplified physically based models, with a view to developing EWSs specifically calibrated for the morpho-climatic features of a wide area.

Acknowledgements The study reported in this paper was carried out within the framework of the project *Grandi frane in roccia e frane superficiali a cinematica rapida in aree montane: metodi per la previsione temporale e spaziale (prediction and susceptibility)*, funded by Dipartimento per gli Affari Regionali e le Autonomie della Presidenza del Consiglio dei Ministri. The authors wish to thank Emanuele Raso for making the monitoring site available, and for providing his support during installation and maintenance of the monitoring system. The authors are also grateful to Jagadish Kundu, a post doc researcher at Dipartimento di Scienze della Terra, Sapienza University of Rome, for his helpful suggestions during the analysis of the data.

Author contributions LS worked on the conceptualization of this paper, data collection, and development of analyses. He also prepared the original draft. MF and GMM. worked on data curation and cooperated in writing, reviewing, and editing the manuscript. MP and GSM coordinated the research group and supervised the research work. They also cooperated in manuscript review and editing.

Funding The study reported in this paper was carried out within the framework of the project “Grandi frane in roccia e frane superficiali a cinematica rapida in aree montane: metodi per la previsione temporale e spaziale (prediction and susceptibility)”, funded by Dipartimento per gli Affari Regionali e le Autonomie della Presidenza del Consiglio dei Ministri.

Declarations

Conflict of interest The authors declare no competing interests.

Open Access This article is licensed under a Creative Commons Attribution 4.0 International License, which permits use, sharing, adaptation, distribution and reproduction in any medium or format, as long as you give appropriate credit to the original author(s) and the source, provide a link to the Creative Commons licence, and indicate if changes were made. The images or other third party material in this article are included in the article’s Creative Commons licence, unless indicated otherwise in a credit line to the material. If material is not included in the article’s Creative Commons licence and your intended use is not permitted by statutory regulation or exceeds the permitted use, you will need to obtain permission directly from the copyright holder. To view a copy of this licence, visit <http://creativecommons.org/licenses/by/4.0/>.

References

- Abraham MT, Satyam N, Pradhan B, Segoni S, Alamri A (2022) Developing a prototype landslide early warning system for Darjeeling Himalayas using SIGMA model and real-time field monitoring. *Geosci J* 26:289–301. <https://doi.org/10.1007/s12303-021-0026-2>
- Abraham M.T., Satyam N., Rosi A., Pradhan B., Segoni S. (2021) Usage of antecedent soil moisture for improving the performance of rainfall thresholds for landslide early warning. *Catena*, 200: 105147, doi: <https://doi.org/10.1016/j.catena.2021.105147>.
- Aleotti P (2004) A warning system for rainfall-induced shallow failures. *Eng Geol* 73:247–265. <https://doi.org/10.1016/j.enggeo.2004.01.007>
- Alfieri L, Salamon P, Pappenberger F, Wetterhall F (2012) Operational early warning systems for water-related hazards in Europe. *Environ Sci Policy* 21:35–49. <https://doi.org/10.1016/j.envsci.2012.01.008>
- An H, Viet TT, Lee GH, Kim Y, Kim M, Noh S, Noh J (2016) Development of time-variant landslide-prediction software considering three-dimensional subsurface unsaturated flow. *Environ Model Softw* 85:172–183. <https://doi.org/10.1016/j.envsoft.2016.08.009>
- Anderson MG, Holcombe E, Blake JR, Ghesquire F, Holm-Nielsen N, Fisseha T (2011) Reducing landslide risk in communities: evidence from the Eastern Caribbean. *Appl Geogr* 31:590–599. <https://doi.org/10.1016/j.apgeog.2010.11.001>
- Ávila FF, Alvalá RC, Mendes RM, Amore DJ (2021) The influence of land use/land cover variability and rainfall intensity in triggering landslides: a back-analysis study via physically based models. *Nat Hazards* 105:1139–1161. <https://doi.org/10.1007/s11069-020-04324-x>

- Badoux A, Graf C, Rhyner J, Kuntner R, McArdell BW (2009) A debris-flow alarm system for the Alpine Illgraben catchment: design and performance. *Nat Hazards* 49:517–539. <https://doi.org/10.1007/s11069-008-9303-x>
- Baum RL, Godt JW, Savage WZ (2010) Estimating the timing and location of shallow rainfall-induced landslides using a model for transient, unsaturated infiltration. *J Geophys Res* 115:F03013. <https://doi.org/10.1029/2009JF001321>
- Baum R.L., Savage W.Z., Godt J.W. (2008) TRIGRS — a Fortran program for transient rainfall infiltration and grid-based regional slope-stability analysis, version 2.0. U.S. Geological Survey Open-File Report 2008–1159: 75 pp.
- Berti M, Martina MLV, Franceschini S, Pignone S, Simoni A, Pizzio M (2012) Probabilistic rainfall thresholds for landslide occurrence using a Bayesian approach. *J Geophys Res Earth Surf* 117:F04006. <https://doi.org/10.1029/2012JF002367>
- Bezák N, Jemec AM, Mikoš M (2019) Application of hydrological modelling for temporal prediction of rainfall-induced shallow landslides. *Landslides* 16:1273–1283. <https://doi.org/10.1007/s10346-019-01169-9>
- Bogaard T, Greco R (2018) Invited perspectives: hydrological perspectives on precipitation intensity–duration thresholds for landslide initiation: proposing hydro-meteorological thresholds. *Nat Hazard* 18:31–39. <https://doi.org/10.5194/nhess-18-31-2018>
- Bordoni M, Meisina C, Valentino R, Lu N, Bittelli M, Chersich S (2015) Hydrological factors affecting rainfall-induced shallow landslides: from the field monitoring to a simplified slope stability analysis. *Eng Geol* 193:19–37. <https://doi.org/10.1016/j.enggeo.2015.04.006>
- Brandolini P, Cevasco A, Capolongo D, Pepe G, Lovergine F, Del Monte M (2018) Response of terraced slopes to a very intense rainfall event and relationships with land abandonment: a case study from Cinque Terre (Italy). *Land Degrad Dev* 29:630–642. <https://doi.org/10.1002/ldr.2672>
- Brunetti MT, Peruccacci S, Rossi M, Luciani S, Valigi D, Guzzetti F (2010) Rainfall thresholds for the possible occurrence of landslides. *Nat Hazard* 10:447–458. <https://doi.org/10.5194/nhess-10-447-2010>
- Cardinali M, Galli M, Guzzetti F, Ardizzone F, Reichenbach P, Bartocchini P (2006) Rainfall induced landslides in December 2004 in Southwestern Umbria, Central Italy. *Nat Hazard* 6:237–260. <https://doi.org/10.5194/nhess-6-237-2006>
- Cevasco A, Francioli G, Robbiano A, Sacchini A, Vincenzi E (2009) Methodological procedures for landslide’s risk mitigation for civil protection purposes in the Genoa municipality area. *Rendiconti Online Societa Geologica Italiana* 6:152–153
- Cevasco A, Brandolini P, Scopesi C, Rellini I (2013) Relationships between geo-hydrological processes induced by heavy rainfall and land-use: the case of 25 October 2011 in the Vernazza catchment (Cinque Terre, NW Italy). *J Maps* 9:289–298. <https://doi.org/10.1080/17445647.2013.780188>
- Cevasco A, Diodato N, Revellino P, Fiorillo F, Grelle G, Guadagno FM (2015) Storminess and geohydrological events affecting small coastal basins in a terraced Mediterranean environment. *Sci Total Environ* 532:208–219. <https://doi.org/10.1016/j.scitotenv.2015.06.017>
- Chen SU, Chou HT, Chen SC, Wu CH, Lin BS (2014) Characteristics of rainfall-induced landslides in Miocene formations: a case study of the Shenmu watershed, Central Taiwan. *Eng Geol* 169:133–146. <https://doi.org/10.1016/j.enggeo.2013.11.020>
- Crosta G (1998) Regionalization of rainfall thresholds: an aid to landslide hazard evaluation. *Environ Geol* 35:131–145. <https://doi.org/10.1007/s002540050300>
- Crosta GB, Frattini P (2003) Distributed modelling of shallow landslides triggered by intense rainfall. *Nat Hazard* 3:81–93. <https://doi.org/10.5194/nhess-3-81-2003>
- Dai FC, Lee CF, Wang SJ (2003) Characterization of rainfall-induced landslides. *Int J Remote Sens* 24:4817–4834. <https://doi.org/10.1080/014311601131000082424>
- Davis G, Ekwue E (2022) Hydrus-1D simulation of two-stage cross-flow pre-filtration of turbid river water. *Water Supply* 22:1244–1254. <https://doi.org/10.2166/ws.2021.355>
- Di Napoli M, Carotenuto F, Cevasco A, Confuorto P, Di Martire D, Firpo M, Pepe G, Raso E, Calcaterra D (2020) Machine learning ensemble modelling as a tool to improve landslide susceptibility mapping reliability. *Landslides* 17:1897–1914. <https://doi.org/10.1007/s10346-020-01392-9>
- Di Napoli M, Di Martire D, Bausilio G, Calcaterra D, Confuorto P, Firpo M, Pepe G, Cevasco A (2021) Rainfall-induced shallow landslide detachment, transit and runout susceptibility mapping by integrating machine learning techniques and GIS-based approaches. *Water* 13:488. <https://doi.org/10.3390/w13040488>
- Dikshit A, Satyam N (2019) Probabilistic rainfall thresholds in Chibo, India: estimation and validation using monitoring system. *Journal of Mountain Sciences* 16:870–883. <https://doi.org/10.1007/s11629-018-5189-6>

- Faccini F, Robbiano A., Raso E., Roccati A. (2013) Gravity-driven deep-reaching deformations and large-scale landslides in recently uplifted mountain areas: the case-study of mt. Cucco and Belpiano (ligurian Apennine, Italy). *Italian Journal of Engineering Geology and Environment Special issue 2013 - International Conference on Vajont—1963–2013—Thoughts and analyses after 50 years since the catastrophic landslide (Padua, Italy—8–10 October 2013):* 141–152. <https://doi.org/10.4408/IJEGE.2013-06.B-11>
- Fredlund DG, Sheng D, Zhao J (2011) Estimation of soil suction from the soil–water characteristic curve. *Can Geotech J* 48:186–198. <https://doi.org/10.1139/T10-060>
- Froese CR, Murray C, Cavers DS, Anderson WS, Bidwell AK, Read RS, Cruden DM, Langenberg W (2005) Development and implementation of a warning system for the South Peak of Turtle Mountain. In: Hungr O, Fell R, Couture R, Eberhardt E (eds) *International conference on landslide risk management*. Taylor & Francis, Vancouver, pp 705–712
- Froude MJ, Petley DN (2018) Global fatal landslide occurrence from 2004 to 2016. *Nat Hazard* 18:2161–2181. <https://doi.org/10.5194/nhess-18-2161-2018>
- Gardner WR (1958) Some steady-state solutions of the unsaturated moisture flow equation with application to evaporation from a water table. *Soil Sci* 85:228–232. <https://doi.org/10.1097/00010694-195804000-00006>
- Gariano SL, Sarkar R, Dikshit A, Dorji K, Brunetti MT, Peruccacci S, Melillo M (2019) Automatic calculation of rainfall thresholds for landslide occurrence in Chukha Dzongkhag, Bhutan. *Bull Eng Geol Env* 78:4325–4332. <https://doi.org/10.1007/s10064-018-1415-2>
- Gariano SL, Melillo M, Peruccacci S, Brunetti MT (2020) How much does the rainfall temporal resolution affect rainfall thresholds for landslide triggering? *Nat Hazards* 100:655–670. <https://doi.org/10.1007/s11069-019-03830-x>
- Genevois R, Tecca PR, Deganutti AM (2018) Debris flow mitigation and control in the Dolomites (north-eastern Italy). *Ital J Eng Geol Environ* 2:57–65. <https://doi.org/10.4408/IJEGE.2018-02.O-04>
- Giannini LM, Varone C, Esposito C, Marmoni GM, Scarascia MG, Schilirò L (2022) Earthquake-induced reactivation of landslides under variable hydrostatic conditions: evaluation at regional scale and implications for risk assessment. *Landslides*. <https://doi.org/10.1007/s10346-022-01882-y>
- Giordan D, Cignetti M, Godone D, Peruccacci S, Raso E, Pepe G, Calcaterra D, Cevasco A, Firpo M, Scarpellini P, Gnone M (2020) A new procedure for an effective management of geo-hydrological risks across the “Sentiero Verde-Azzurro” Trail, Cinque Terre National Park, Liguria (North-Western Italy). *Sustainability* 12:561. <https://doi.org/10.3390/su12020561>
- Govi M, Mortara G, Sorzana P (1985) Eventi idrologici e frane. *Geologia Applicata e Idrogeologia* 20:359–375
- Guzzetti F, Tonelli G (2004) Information system on hydrological and geomorphological catastrophes in Italy (SICI): a tool for managing landslide and flood hazards. *Nat Hazard* 4:213–232. <https://doi.org/10.5194/nhess-4-213-2004>
- Guzzetti F, Cardinali M, Reichenbach P (1994) The AVI Project: a bibliographical and archive inventory of landslides and floods in Italy. *Environ Manage* 18:623–633. <https://doi.org/10.1007/BF02400865>
- Guzzetti F, Peruccacci S, Rossi M, Stark CP (2007) Rainfall thresholds for the initiation of landslides in central and southern Europe. *Meteorol Atmos Phys* 98:239–267. <https://doi.org/10.1007/s00703-007-0262-7>
- Guzzetti F, Peruccacci S, Rossi M, Stark CP (2008) The rainfall intensity-duration control of shallow landslides and debris-flows: an update. *Landslides* 5:3–17. <https://doi.org/10.1007/s10346-007-0112-1>
- Haque U, Blum P, Da Silva P, Andersen P, Pilz JC, Sergey R, Malet JP, Jemec AM, Andres N, Poyiadji E, Lamas PC, Zhang W, Peshevski I, Pétursson HG, Kurt T, Dobrev N, García-Davalillo JC, Halkia M, Ferri S, Gaprindashvili G, Engström J, Keelling D (2016) Fatal landslides in Europe. *Landslides* 13:1545–1554. <https://doi.org/10.1007/s10346-016-0689-3>
- Haque U, da Silva PF, Devoli G, Pilz J, Zhao B, Khaloua A, Wilopo W, Andersen P, Lu P, Lee J, Yamamoto T, Keellings D, Wu JH, Glass GE (2019) The human cost of global warming: deadly landslides and their triggers (1995–2014). *Sci Total Environ* 682:673–684. <https://doi.org/10.1016/j.scitotenv.2019.03.415>
- Hsu YC, Liu KF (2019) Combining TRIGRS and DEBRIS-2D models for the simulation of a rainfall infiltration induced shallow landslide and subsequent debris flow. *Water* 11:890. <https://doi.org/10.3390/w11050890>
- Huang J, Ju NP, Liao YJ, Liu DD (2015) Determination of rainfall thresholds for shallow landslides by a probabilistic and empirical method. *Nat Hazard* 15:2715–2723. <https://doi.org/10.5194/nhess-15-2715-2015>
- Hungr O, Leroueil S, Picarelli L (2014) The Varnes classification of landslide types, an update. *Landslides* 11:167–194. <https://doi.org/10.1007/s10346-013-0436-y>

- Intrieri E, Gigli G, Mugnai F, Fanti R, Casagli N (2012) Design and implementation of a landslide early warning system. *Eng Geol* 147–148:124–136. <https://doi.org/10.1016/j.enggeo.2012.07.017>
- Iverson RM (2000) Landslide triggering by rain infiltration. *Water Resour Res* 36:1897–1910. <https://doi.org/10.1029/2000WR900090>
- Jensen DT, Hargreaves GH, Temesgen B, Allen RG (1997) Computation of ET_o under nonideal conditions. *J Irrig Drain Eng* 123:394–400. [https://doi.org/10.1061/\(ASCE\)0733-9437\(1997\)123:5\(394\)](https://doi.org/10.1061/(ASCE)0733-9437(1997)123:5(394))
- Jeong S, Lee K, Kim J, Kim Y (2017) Analysis of rainfall-induced landslide on unsaturated soil slopes. *Sustainability* 9:1280. <https://doi.org/10.3390/su9071280>
- Kanzari S, Ben NB, Ben MS, Rezig M (2018) Hydrus-1D model calibration and validation in various field conditions for simulating water flow and salts transport in a semi-arid region of Tunisia. *Sustain Environ Res* 28:350–356. <https://doi.org/10.1016/j.serj.2018.10.001>
- Kemmer G, Keller S (2010) Nonlinear least-squares data fitting in Excel spreadsheets. *Nat Protoc* 5:267–281. <https://doi.org/10.1038/nprot.2009.182>
- Kirschbaum D, Adler R, Adler D, Peters-Lidard C, Huffman G (2012) Global distribution of extreme precipitation and high impact landslides in 2010 relative to previous years. *J Hydrometeorol* 13:1536–1551. <https://doi.org/10.1175/JHM-D12-02.1>
- Kristo C, Rahardjo H, Satyanaga A (2019) Effect of hysteresis on the stability of residual soil slope. *Int Soil Water Conserv Res* 7:226–238. <https://doi.org/10.1016/j.iswcr.2019.05.003>
- Liao Z, Hong Y, Kirschbaum D, Liu C (2011) Assessment of shallow landslides from Hurricane Mitch in central America using a physically based model. *Environ Earth Sci* 66:1697–1705. <https://doi.org/10.1007/s12665-011-0997-9>
- Regione Liguria (2012) Ambiente in Liguria: catalogo banche dati [database]. Genova (Italy): Regione Liguria. <http://www.banchedati.ambienteinliguria.it/index.php/aria/meteo> (last access: 10 May 2021)
- Likos WJ, Lu N, Godt JW (2013) Hysteresis and uncertainty in soil–water retention curve parameters. *J Geotech Geoenviron Eng* 140:04013050. [https://doi.org/10.1061/\(ASCE\)GT.1943-5606.0001071](https://doi.org/10.1061/(ASCE)GT.1943-5606.0001071)
- Lu N, Godt J (2008) Infinite slope stability under steady unsaturated seepage conditions. *Water Resour Res* 44:W11404. <https://doi.org/10.1029/2008WR006976>
- Lu N, Likos WJ (2006) Suction stress characteristic curve for unsaturated soil. *J Geotech Geoenviron Eng* 132:131–142. [https://doi.org/10.1061/\(ASCE\)1090-0241\(2006\)132:2\(131\)](https://doi.org/10.1061/(ASCE)1090-0241(2006)132:2(131))
- Lu N, Godt JW, Wu DT (2010) A closed-form equation for effective stress in unsaturated soil. *Water Resour Res* 46:W05515. <https://doi.org/10.1029/2009WR008646>
- Lu N, Godt JW (2013) Hillslope hydrology and stability. Cambridge University Press, Cambridge. <https://doi.org/10.1017/CBO9781139108164>
- Marc O, Stumpf A, Malet JP, Gosset M, Uchida T, Hao CS (2018) Initial insights from a global database of rainfall-induced landslide inventories: the weak influence of slope and strong influence of total storm rainfall. *Earth Surf Dyn* 6:903–922. <https://doi.org/10.5194/esurf-6-903-2018>
- Martini S., Pesce G., De Franchi R. (2004) Manual for dry walls' construction: guidelines for the maintenance of terraces in Cinque Terre (in Italian). <http://db.parks.it/pdf/situufficiali/PN5TRdocum ento-7-1.pdf>. Access 10 May 2021
- Martino S, Marmoni GM, Fiorucci M, Ceci AF, Discenza ME, Rouhi J, Tedoradze D (2022) Role of antecedent rainfall in the earthquake-triggered shallow landslides involving unsaturated slope covers. *Appl Sci* 12:2917. <https://doi.org/10.3390/app12062917>
- Maskrey A (2011) Revisiting community-based disaster risk management. *Environ Hazards* 10:42–52. <https://doi.org/10.3763/ehaz.2011.0005>
- Mathew J, Babu DG, Kundu S, Kumar KV, Pant CC (2014) Integrating intensity-duration-based rainfall threshold and antecedent rainfall-based probability estimate towards generating early warning for rainfall-induced landslides in parts of the Garhwal Himalaya, India. *Landslides* 11:575–588. <https://doi.org/10.1007/s10346-013-0408-2>
- Merritt WS, Letcher RA, Jakeman AJ (2003) A review of erosion and sediment transport models. *Environ Model Softw* 18:761–799. [https://doi.org/10.1016/S1364-8152\(03\)00078-1](https://doi.org/10.1016/S1364-8152(03)00078-1)
- Mirus BB, Becker RE, Baum RL, Smith JB (2018) Integrating real-time subsurface hydrologic monitoring with empirical rainfall thresholds to improve landslide early warning. *Landslides* 15:1909–1919. <https://doi.org/10.1007/s10346-018-0995-z>
- Papa M.N., Medina V., Bateman A. (2011) Derivation of critical rainfall thresholds for debris flow warnings through mathematical and numerical modeling. *Italian Journal of Engineering Geology and Environment*, Special issue 2011—5th International conference on debris-flow hazards mitigation: mechanics, prediction and assessment. Padua, June 14th–17th, 2011: 495–502. <https://doi.org/10.4408/IJEGE.2011-03.B-055>

- Park HJ, Lee JH, Woo LK (2013) Assessment of rainfall-induced shallow landslide susceptibility using a GIS-based probabilistic approach. *Eng Geol* 161:1–15. <https://doi.org/10.1016/j.enggeo.2013.04.011>
- Park HJ, Jang JY, Lee JH (2019) Assessment of rainfall-induced landslide susceptibility at the regional scale using a physically based model and fuzzy-based Monte Carlo simulation. *Landslides* 16:695–713. <https://doi.org/10.1007/s10346-018-01125-z>
- Pasuto A, Silvano S (1998) Rainfall as a trigger of shallow mass movements. A case study in the Dolomites. *Italy Environ Geol* 35:184–189. <https://doi.org/10.1007/s002540050304>
- Pedemonte R. (2005) Contributo alla classificazione dei climi della Liguria – distribuzione geografica delle precipitazioni annue, IV parte. *Rivista Ligure di Meteorologia*. http://www.nimbus.it/liguria/rlm15/clima_liguria.htm. Access 10 May 2021
- Pepe G, Baudinelli E, Zanini M, Calcaterra D, Cevasco A, Scarpellini P, Firpo M (2020) Application of bioengineering techniques as geo-hydrological risk mitigation measures in a highly valuable cultural landscape: experiences from the Cinque Terre National Park (Italy). *Sustainability* 12:8653. <https://doi.org/10.3390/su12208653>
- Petley D (2012) Global patterns of loss of life from landslides. *Geology* 40:927–930. <https://doi.org/10.1130/g33217.1>
- Rahardjo H, Kim Y, Satyanaga A (2019) (2019) Role of unsaturated soil mechanics in geotechnical engineering. *Int J Geo-Eng* 10:8. <https://doi.org/10.1186/s40703-019-0104-8>
- Raso E, Cevasco A, Di Martire D, Pepe G, Scarpellini P, Calcaterra D, Firpo M (2019) Landslide-inventory of the Cinque Terre National Park (Italy) and quantitative interaction with the trail network. *J Maps* 15:818–830. <https://doi.org/10.1080/17445647.2019.1657511>
- Rosso R, Rulli MC, Vannucchi G (2006) A physically based model for the hydrologic control on shallow landsliding. *Water Resour Res* 42:W06410. <https://doi.org/10.1029/2005WR004369>
- Sajinkumar KS, Anbazhagan S (2015) Geomorphic appraisal of landslides on the windward slope of Western Ghats, southern India. *Nat Hazards* 75:953–973. <https://doi.org/10.1007/s11069-014-1358-2>
- Schilirò L, Cevasco A, Esposito C, Scarascia MG (2018) Shallow landslide initiation on terraced slopes: inferences from a physically based approach. *Geomat Nat Haz Risk* 9:295–324. <https://doi.org/10.1080/19475705.2018.1430066>
- Schilirò L, Poueme DG, Esposito C, Scarascia MG (2019) The Role of initial soil conditions in shallow landslide triggering: insights from physically based approaches. *Geofluids* 2019:2453786. <https://doi.org/10.1155/2019/2453786>
- Schilirò L, Cepeda JM, Devoli G, Piciullo L (2021) Regional analyses of rainfall-induced landslide initiation in Upper Gudbrandsdalen (South-Eastern Norway) using TRIGRS model. *Geosciences* 11:35. <https://doi.org/10.3390/geosciences11010035>
- Schilirò L., Cevasco A., Esposito C., Scarascia Mugnozza G. (2017) Role of land use in landslide initiation on terraced slopes: inferences from numerical modelling. In: Mikoš M., Casagli N., Yin Y., Sassa K. (eds.) *Advancing culture of living with landslides*. WLF 2017. Springer, Cham: 315–320. https://doi.org/10.1007/978-3-319-53485-5_36
- Shekhar S, Mailapalli DR, Raghuvanshi NS, Sankar DB (2019) Hydrus-1D model for simulating water flow through paddy soils under alternate wetting and drying irrigation practice. *Paddy Water Environ*, 18:73–85. <https://doi.org/10.1007/s10333-019-00765-8>
- Šimůnek J., Šejna M., Saito H., Sakai M., van Genuchten M.Th. (2008) The HYDRUS-1D software package for simulating the movement of water, heat, and multiple solutes in variably saturated media, version 4.0: HYDRUS Software Series 3. Department of Environmental Sciences, University of California Riverside, Riverside, CA.
- Stähli M., Bartelt P. (2007) Von der Auslösung zur Massenbewegung. In: Hegg C., Rhyner J. (eds.) *Warnung bei aussergewöhnlichen Naturereignissen*: 33–38
- Thiebes B, Bell R, Glade T, Jäger S, Mayer J, Anderson M, Holcombe L (2014) Integration of a limit-equilibrium model into a landslide early warning system. *Landslides* 11:859–875. <https://doi.org/10.1007/s10346-013-0416-2>
- Tran TV, Alvioli M, Hoang VH (2022) (2022) Description of a complex, rainfall-induced landslide within a multi-stage three-dimensional model. *Nat Hazards* 110:1953–1968. <https://doi.org/10.1007/s11069-021-05020-0>
- Tufano R, Cesarano M, Fusco F, De Vita P (2019) Probabilistic approaches for assessing rainfall thresholds triggering shallow landslides. The study case of the peri-Vesuvian area (southern Italy). *Italian J Eng Geol Environ Special Issue* 1–2019:105–110. <https://doi.org/10.4408/IJEGE.2019-01.S-17>
- Valenzuela P, Zêzere JL, Domínguez-Cuesta MJ, Mora García MA (2019) Empirical rainfall thresholds for the triggering of landslides in Asturias (NW Spain). *Landslides* 16:1285–1300. <https://doi.org/10.1007/s10346-019-01170-2>

- van Genuchten M, Th. (1980) A closed-form equation for predicting the hydraulic conductivity of unsaturated soils. *Soil Sci Soc Am J* 44:892–898. <https://doi.org/10.2136/sssaj1980.03615995004400050002x>
- Vanapalli SK, Fredlund DG (2000) Comparison of different procedures to predict unsaturated soil shear strength. In: Shackelford CD, Houston SL, Chang NY (Eds) *Advances in unsaturated geotechnics*. Society of Civil Engineers
- Weidner L, Oommen T, Escobar-Wolf R, Sajinkumar KS, Samuel RA (2018) Regional-scale back-analysis using TRIGRS: an approach to advance landslide hazard modeling and prediction in sparse data regions. *Landslides* 15:2343–2356. <https://doi.org/10.1007/s10346-018-1044-7>
- Wilson RC, Wieczorek GF (1995) Rainfall thresholds for the initiation of debris flow at La Honda, California. *Environ Eng Geosci* 1:11–27. <https://doi.org/10.2113/gseegeosci.1.1.11>
- Yang Z, Cai H, Shao W, Huang D, Uchimura T, Lei X, Tian H, Qiao J (2019) Clarifying the hydrological mechanisms and thresholds for rainfall-induced landslide: in situ monitoring of big data to unsaturated slope stability analysis. *Bull Eng Geol Env* 78:2139–2150. <https://doi.org/10.1007/s10064-018-1295-5>

Publisher's Note Springer Nature remains neutral with regard to jurisdictional claims in published maps and institutional affiliations.